Research Article | Vol. 33, No. 21 / 20 Oct 2025 / *Optics Express* 43665

Optics EXPRESS

Amplifier enhanced gain-through-filtering instability in a hybrid Kerr cavity

MINJI SHI,[1,†] STEFANO NEGRINI,[2,†] NICOLAS ENGLEBERT,[3] FRANÇOIS LEO,[4] MATTEO CONFORTI,[2] ARNAUD MUSSOT,[2] AND AURO M. PEREGO[1,*]

[1] *Aston Institute of Photonic Technologies, Aston University, Birmingham B4 7ET, United Kingdom*
[2] *University of Lille, CNRS, UMR 8523-PhLAM Physique des Lasers Atomes et Molécules, F- 59000 Lille, France*
[3] *Department of Electrical Engineering, California Institute of Technology, Pasadena, California 91125, USA*
[4] *Service OPERA-Photonique, Université libre de Bruxelles (ULB), Brussels, Belgium*
[†] These authors contributed equally to this work.
[*] *a.perego1@aston.ac.uk*

Abstract: We investigate analytically, numerically and experimentally the gain-through-filtering modulation instability in a hybrid driven Kerr cavity in the normal dispersion regime including an erbium-doped fiber amplifier. We show that, thanks to the increased cavity finesse enabled by the intracavity optical gain, the injection power threshold for the modulation instability can be substantially reduced, and the energy transfer to spectral sidebands enhanced. Our findings demonstrate how to improve efficiency and bandwidth in optical frequency comb generation based on the gain-through-filtering modulation instability.

1. Introduction

Optical frequency combs (OFCs), optical rulers consisting of coherent laser spectral lines equally spaced in frequency, are of vital importance in various scientific and technological domains owing to their wide range of applications including in spectroscopy, microscopy, sensing, optical clocks, astronomy, telecomunications and more [1,2]. OFCs can be generated by a variety of platforms including mode-locked lasers [3], electro-optic modulators [4], and driven resonators – both micro [5] and fiber ones [6]. Fiber resonators have historically provided an important playground for the development of OFC generation techniques later adapted to microresonators – e.g. the formation of cavity solitons [7] – and in particular geometries they can achieve quality (Q)-factors of the order of several millions enabling OFC generation both in the the single [8–11] and multimode [12] operational regime too. In the context of fiber resonators, recent methodology, called gain-through-filtering (GTF), has been developed to enable the generation of tunable repetition rate OFCs within passive-driven fiber cavities [13,14]. This technique is built on previous investigation of modulation instabilities (MIs) induced by asymmetric spectral filtering in nonlinear optical systems [13]. The approach leverages the phase contribution of a filter to achieve perfect phase matching between a strong pump and weak sidebands in the normal dispersion regime of a ring cavity. As a result, MI can be triggered, leading to the generation of two symmetric sidebands around the pump, with one positioned close to the filter. So far GTF induced OFCs have been demonstrated in ring fiber resonators, where, due to the low finesse, a significant large amount of pump power is required to cross the MI threshold. Inspired by the recent progress in hybrid active-passive fiber ring cavities (without filter) for generating low background cavity solitons [15,16], we investigate in this work the impact of

#579357 https://doi.org/10.1364/OE.579357
Journal © 2025 Received 17 Sep 2025; accepted 19 Sep 2025; published 6 Oct 2025

Optics EXPRESS

optical amplification on the GTF process through the inclusion of an intracavity erbium-doped fiber amplifier (EDFA). We updated the theoretical model presented in [14] to consider the amplifier contribution developing a formalism suitable for analytical and numerical investigation of the GTF process in an active-passive fiber resonator. These theoretical development are confirmed through experimental observations with a very good agreement. The intracavity amplifier improves the conversion efficiency from the pump to the OFC sidebands resulting in a reduced input pump power MI threshold.

2. Ikeda map model

We consider a ring cavity, which is illustrated in Fig. 1 (a), consisting of four components : an EDFA, a dispersion-shifted fiber (DSF, $\beta_2>0$ at the driving frequency), a narrowband filter and a fiber coupler. The boundary conditions (BCs) of the Ikeda map model read: [14]

$$A_{n+1}(z=0,t) = \rho e^{i\varphi_0} h(t) \star A_n(z=L,t) + \theta\sqrt{P_{\mathrm{in}}}. \tag{1}$$

Here, $A_n(z,t)$ represents the slowly varying envelope of the electric field. The variable t corresponds to the retarded time, while z denotes the spatial coordinate along the fiber ring cavity. The variable n indicates the roundtrip number, and P_{in} signifies the injected pump power. The parameters ρ and θ are the reflection and transmission coefficients of the coupler for field respectively. Additionally, φ_0 represents the linear phase shift accumulated over one roundtrip, modulo 2π. The symbol $\star$ denotes convolution, and $h(t)$ is the filter impulse response, which has a frequency-domain counterpart referred to as the filter transfer function, i.e., $H(\Omega) = \int_{-\infty}^{\infty} h(t)e^{i\Omega t}$. In this paper, we consider a higher-order Lorentzian filter, characterized by its transfer function given by

$$H(\Omega) = e^{F(\Omega)+i\psi(\Omega)}, \tag{2a}$$

$$F(\Omega) = b\frac{a^4}{(\Omega-\Omega_f)^4 + a^4}, \tag{2b}$$

$$\psi(\Omega) = ba\frac{(\Omega-\Omega_f)[(\Omega-\Omega_f)^2 + a^2]}{\sqrt{2}[(\Omega-\Omega_f)^4 + a^4]}. \tag{2c}$$

Here, a is related to the filter bandwidth at full width at half maximum (in rad/ns), $b<0$ is a dimensionless parameter that governs the filter strength, specifically the maximum attenuation, and Ω_f represents the filter frequency detuning with respect to the resonator pump frequency. The profiles of amplitude and phase of $H(\Omega)$ are illustrated in Fig. 1(b) with parameters compatible with the ones used in experimental setup (see section 4). We notice that $\psi(\Omega) \neq 0$ at $\Omega = 0$, which introduces an additional linear phase for each roundtrip, resulting in a linear detuning of $\varphi_0' = \varphi_0 + \psi(0)$.

The propagation of light waves in the EDFA and DSF is governed by the following equations, respectively:

$$0 \le z \le L_1 : \quad \frac{\partial A_n}{\partial z} = \left(\frac{g}{2} + \frac{g}{2\Omega_g^2}\frac{\partial^2}{\partial t^2} - i\frac{\beta_2^{(1)}}{2}\frac{\partial^2}{\partial t^2} + i\gamma^{(1)}|A_n|^2\right)A_n, \tag{3}$$

$$L_1 < z \le L : \quad \frac{\partial A_n}{\partial z} = \left(-i\frac{\beta_2^{(2)}}{2}\frac{\partial^2}{\partial t^2} + i\gamma^{(2)}|A_n|^2\right)A_n. \tag{4}$$

Here, 1 and 2 indices label the EDFA and the passive fiber, respectively, and we denote the total cavity length as $L = L_1 + L_2$. $\beta_2^{(1),(2)}$ are the group velocity dispersion values, and $\gamma^{(1),(2)}$ are the Kerr nonlinearity coefficients. Ω_g is the angular frequency bandwidth of the gain. The EDFA

Optics EXPRESS

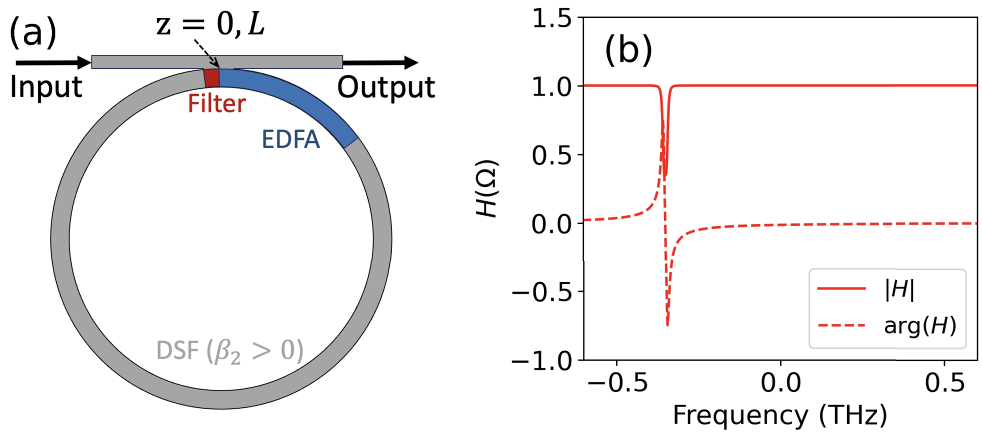

Fig. 1. (a) Setup schematic: a fiber ring cavity made of an amplifier (EDFA), a passive fiber with normal dispersion (DSF) and a filter. (b) Profiles of amplitude and phase of the filter transfer function $H(\Omega)$. Parameters used are $a = 43$ rad/ns, $b = -1.06$ and $\Omega_f/(2\pi) = -0.35$ THz.

gain is modeled as in [15,17] with $g(z) = \frac{g_0}{1+(P_{\text{sat}}t_R)^{-1}\int_0^{t_R}|A_n(z,t)|^2dt}$, and g_0 denoting the unsaturated gain, P_{sat} being the gain saturation power, and t_R being the roundtrip time.

In the scenario involving a short pulse of duration t_D compared to the round trip time, the term $(P_{\text{sat}}t_R)^{-1}\int_0^{t_R}|A_n(L_1,t)|^2dt$ can be approximated by an integral over a certain time window, i.e., $\frac{r_D}{P_{\text{sat}}}t_W^{-1}\int_{t_W}|A_n(L_1,t)|^2dt$, where t_W is the width of the simulation time window, $r_D \equiv t_D/t_R \ll 1$, and $\int_{t_W}$ represents the integral over t_w. Hence we obtain $g = \frac{g_0}{1+(P_{\text{sat}}t_W)^{-1}\int_{t_W} r_D|A_n(L_1,t)|^2dt}$.

The stationary quasi continuous wave (CW) solution of the cavity is given by $A_n(z) = \sqrt{P_n(z)}e^{i\phi_n(z)}$ with real amplitude $\sqrt{P_n(z)}$ and phase $\phi_n(z)$. Then the gain reads $g = \frac{P_{\text{sat}}}{P_{\text{sat}}+r_DP_n(L_1)}g_0$, depending on the ratio r_D, and P_n and ϕ_n can be obtained by solving Eqs. (3) and (4), which yields

$$0 \le z \le L_1: \quad P_n(z) = P_n(0)e^{gz},\ \phi_n(z) = \phi_n(0) + \gamma^{(1)}P_n(0)\frac{1}{g}(e^{gz}-1), \tag{5}$$

$$;L_1 < z \le L: \quad P_n(z) = P_n(L_1),\ \phi_n(z) = \phi_n(L_1) + \gamma^{(2)}(z-L_1)P_n(L_1), \tag{6}$$

leading to

$$P_n(L) = P_n(0)e^{gL_1}, \tag{7}$$

$$\phi_n(L) = \phi_n(0) + \gamma^{(1)}P_n(0)\frac{1}{g}(e^{gL_1}-1) + \gamma^{(2)}P_n(0)L_2e^{gL_1}. \tag{8}$$

Considering the boundary condition for the steady solution, we obtain

$$A_{n+1}(0) = \rho e^{i\varphi_0}H(0)A_n(L) + \theta\sqrt{P_{\text{in}}}. \tag{9}$$

Finally, the requirement $A_{n+1}(0) = A_n(0)$ yields the implicit form of the steady solution:

$$\sqrt{P(0)} - \sqrt{P(0)}\mu e^{i\nu} = \theta\sqrt{P_{\text{in}}}e^{-i\phi(0)} \tag{10}$$

where $\mu = \rho e^{\frac{gL_1}{2}+F(0)}$ and $\nu = \varphi_0' + \gamma^{(1)}P(0)\frac{1}{g}(e^{gL_1}-1) + \gamma^{(2)}P(0)L_2e^{gL_1} = \varphi_0' + \gamma^{(1)}P(L_1)\frac{1}{g}(1 - e^{-gL_1}) + \gamma^{(2)}P(L_1)L_2$. Taking the square modulus of both sides of Eq. (10), we obtain

$$P(L_1)e^{-gL_1}\left[1 + \mu^2 - 2\mu\cos\nu\right] = \theta^2P_{\text{in}}, \tag{11}$$

by which the intracavity power $P(L_1)$ can be solved. The relation between the injection and the intracavity power is shown in Fig. 2.

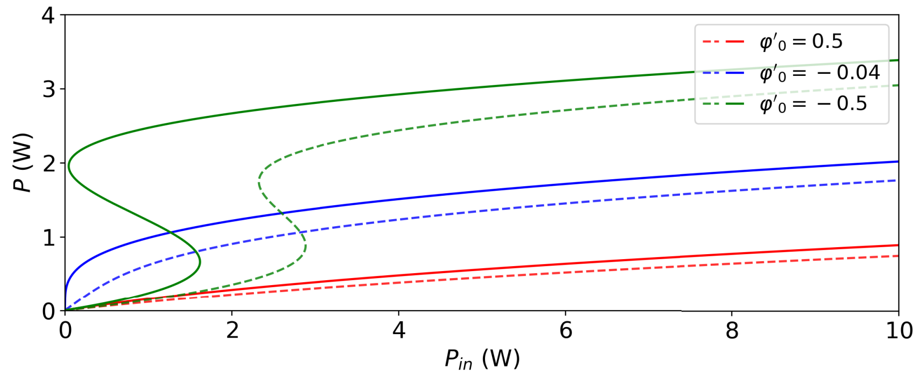

Fig. 2. Relation between input and intracavity power calculated by Ikeda map with EDFA (solid lines) and without EDFA (dashed lines). Parameters used are $\rho = \sqrt{0.65}$, $\theta = \sqrt{0.03}$, $g_0 = 4.87$ dB/m, $P_{\rm sat} = 500$mW, $r_D = 1.3/451$, $\gamma^{(1)} = 1.3$ W^{-1}km^{-1}, $\gamma^{(2)} = 3$ W^{-1}km^{-1}, $L_1 = 0.33$ m, $L_2 = 85$ m, and $a = 43$ rad/ns, $b = -1.06$ and $\Omega_f/(2\pi) = -0.35$ THz.

If we assume that the nonlinear phase shift is small compared to the linear phase φ'_0, Eq. (10) yields the following power relation:

$$P(0) \approx \frac{\theta^2 P_{\rm in}}{\left|1-\rho' e^{i\varphi'_0}\right|^2} = \frac{\theta^2 P_{\rm in}}{1+\rho'^2 - 2\rho' \cos\varphi'_0}, \tag{12}$$

where we have defined $\rho' = \rho e^{\frac{gL_1}{2}+F(0)}$. The maximum power is achieved when $\varphi'_0 = 2k\pi$, and is given by $P(0) = \frac{\theta^2 P_{\rm in}}{(1-\rho')^2}$. Consequently, we seek a value of φ'_0 that results in half-maximum power, i.e.,

$$\frac{\theta^2 P_{\rm in}}{1+\rho'^2 - 2\rho' \cos\varphi'_0} = \frac{1}{2}\frac{\theta^2 P_{\rm in}}{(1-\rho')^2}. \tag{13}$$

If we focus exclusively on values of φ'_0 that are near 0, we can approximate $\cos\varphi'_0$ using the expression $1 - \frac{\varphi'^2_0}{2}$. This results in $\varphi'_0 = \pm\frac{1-\rho'}{\sqrt{\rho'}}$. Thus the full width of φ'_0 at half-maximum power is $\frac{2(1-\rho')}{\sqrt{\rho'}}$, and the finesse of the ring cavity reads

$$\mathcal{F} = \frac{\pi\sqrt{\rho'}}{1-\rho'}. \tag{14}$$

3. Modulation instability analysis

To study the stability of the steady state, we consider the following *ansatz*:

$$A_n(z,t) = \left[\sqrt{P(z)} + \eta_n(z,t)\right] e^{i\phi(z)}, \tag{15}$$

where $P(z)$ and $\phi(z)$ are the power and phase of the steady state respectively, $\eta_n(z,t)$ is the perturbation and $|\eta_n(z,t)| \ll \sqrt{P(z)}$. Substituting Eq. (15) into Eq. (1), Eq. (3), and Eq. (4),

Optics EXPRESS

respectively, we derive the equations for $\eta_n(z,t)$, as follows:

$$\text{BC}: \quad \eta_{n+1}(0,t) = \rho e^{i[\varphi_0+\phi_n(L)]} h(t) \star \eta_n(L,t), \tag{16}$$

$$0 \le z \le L_1: \quad \frac{\partial \eta_n}{\partial z} = \frac{g}{2}\left(1 + \frac{1}{\Omega_g^2}\frac{\partial^2}{\partial t^2}\right)\eta_n - i\frac{\beta_2^{(1)}}{2}\frac{\partial^2 \eta_n}{\partial t^2} + i\gamma^{(1)} P(z)(\eta_n + \eta_n^*), \tag{17}$$

$$L_1 < z \le L: \quad \frac{\partial \eta_n}{\partial z} = -i\frac{\beta_2^{(2)}}{2}\frac{\partial^2 \eta_n}{\partial t^2} + i\gamma^{(2)} P(z)(\eta_n + \eta_n^*), \tag{18}$$

where we assumed that the gain is not affected by the small perturbation so that $g = \frac{P_{\text{sat}}}{P_{\text{sat}}+r_D P_n(L_1)} g_0$. If we separate the real and imaginary parts of the perturbation as $\eta_n = a_n + ib_n$, and denote their Fourier counterparts by $\hat{a}_n(z,\Omega)$ and $\hat{b}_n(z,\Omega)$, respectively (where Ω represents the frequency detuning from the pump), we obtain the evolution equation for $(\hat{a}_n, \hat{b}_n)^T$ as follows:

$$\begin{aligned} \text{BC}: \quad & \begin{pmatrix} \hat{a}_{n+1}(0,t) \\ \hat{b}_{n+1}(0,t) \end{pmatrix} = \mathcal{N}_{\text{BC}} \begin{pmatrix} \hat{a}_n(L,t) \\ \hat{b}_n(L,t) \end{pmatrix} \\ & = \rho \begin{pmatrix} \cos[\varphi_0 + \phi_n(L) - \phi_n(0)] & -\sin[\varphi_0 + \phi_n(L) - \phi_n(0)] \\ \sin[\varphi_0 + \phi_n(L) - \phi_n(0)] & \cos[\varphi_0 + \phi_n(L) - \phi_n(0)] \end{pmatrix} \begin{pmatrix} H_+ & -H_- \\ H_- & H_+ \end{pmatrix} \begin{pmatrix} \hat{a}_n(L,t) \\ \hat{b}_n(L,t) \end{pmatrix} \end{aligned} \tag{19}$$

$$0 \le z \le L_1: \quad \frac{\partial}{\partial z}\begin{pmatrix} \hat{a}_n \\ \hat{b}_n \end{pmatrix} = M_1 \begin{pmatrix} \hat{a}_n \\ \hat{b}_n \end{pmatrix} = \left[\frac{g}{2}\left(1 - \frac{\Omega^2}{\Omega_g^2}\right) + \begin{pmatrix} 0 & -\frac{\beta_2^{(1)}\Omega^2}{2} \\ \frac{\beta_2^{(1)}\Omega^2}{2} + 2\gamma^{(1)}P(z) & 0 \end{pmatrix}\right]\begin{pmatrix} \hat{a}_n \\ \hat{b}_n \end{pmatrix}, \tag{20}$$

$$L_1 < z \le L: \quad \frac{\partial}{\partial z}\begin{pmatrix} \hat{a}_n \\ \hat{b}_n \end{pmatrix} = M_2 \begin{pmatrix} \hat{a}_n \\ \hat{b}_n \end{pmatrix} = \begin{pmatrix} 0 & -\frac{\beta_2^{(2)}\Omega^2}{2} \\ \frac{\beta_2^{(2)}\Omega^2}{2} + 2\gamma^{(2)}P(z) & 0 \end{pmatrix}\begin{pmatrix} \hat{a}_n \\ \hat{b}_n \end{pmatrix}, \tag{21}$$

where we introduced the evolution matrix $M_{1,2}$ and the boundary condition matrix $\mathcal{N}_{\text{BC}}$. Here H_+ and H_- are the Fourier transform of the even and odd part of the response function $h(t)$ respectively, which can be evaluated by the following formulae:

$$H_+(\Omega) = \int \frac{h(t) + h^*(t)}{2} e^{i\Omega t} dt = \frac{H(\Omega) + H^*(-\Omega)}{2} \tag{22a}$$

$$H_-(\Omega) = \int \frac{h(t) - h^*(t)}{2i} e^{i\Omega t} dt = \frac{H(\Omega) - H^*(-\Omega)}{2i}. \tag{22b}$$

The perturbations in the same roundtrip at $z = L$ and at $z = 0$ are related by

$$\begin{pmatrix} \hat{a}_n(L) \\ \hat{b}_n(L) \end{pmatrix} = \mathcal{N}_{\text{evo}} \begin{pmatrix} \hat{a}_n(0) \\ \hat{b}_n(0) \end{pmatrix} = e^{\int_{L_1}^{L} M_2(z)dz} e^{\int_0^{L_1} M_1(z)dz} \begin{pmatrix} \hat{a}_n(0) \\ \hat{b}_n(0) \end{pmatrix}, \tag{23}$$

where we have introduced the transformation matrix $\mathcal{N}_{\text{evo}}$ induced by the propagation in EDFA and fiber for one roundtrip, and adopted the integral approximation, which holds under the assumption that $M_{1,2}(z)$ do not vary too rapidly along z. As the two integrals read

Optics EXPRESS

$\int_0^{L_1} P(z)dz = P(0)(e^{gL_1} - 1)/g = P(L_1)(1 - e^{-gL_1})/g$ and $\int_{L_1}^{L} P(z)dz = P(L_1)L_2$ respectively, we obtain

$$\mathcal{N}_{\text{evo}} = e^{\left(1-\frac{\Omega^2}{\Omega_g^2}\right)\frac{gL_1}{2}} \begin{pmatrix} \cos(k_2L_2) & -\frac{\beta_2^{(2)}\Omega^2}{2k_2}\sin(k_2L_2) \\ \frac{2k_2}{\beta_2^{(2)}\Omega^2}\sin(k_2L_2) & \cos(k_2L_2) \end{pmatrix} \begin{pmatrix} \cos(k_1L_1) & -\frac{\beta_2^{(1)}\Omega^2}{2k_1}\sin(k_1L_1) \\ \frac{2k_1}{\beta_2^{(1)}\Omega^2}\sin(k_1L_1) & \cos(k_1L_1) \end{pmatrix}, \tag{24}$$

where $k_1 = \sqrt{\frac{\beta_2^{(1)}\Omega^2}{2}\left[\frac{\beta_2^{(1)}\Omega^2}{2} + \frac{2\gamma^{(1)}(1-e^{-gL_1})P(L_1)}{gL_1}\right]}$ and $k_2 = \sqrt{\frac{\beta_2^{(2)}\Omega^2}{2}\left[\frac{\beta_2^{(2)}\Omega^2}{2} + 2\gamma^{(2)}P(L_1)\right]}$, and

$$\mathcal{N}_{\text{BC}} = \rho \begin{pmatrix} \cos(\Delta\varphi) & -\sin(\Delta\varphi) \\ \sin(\Delta\varphi) & \cos(\Delta\varphi) \end{pmatrix} \begin{pmatrix} H_+ & -H_- \\ H_- & H_+ \end{pmatrix}, \tag{25}$$

with $\Delta\varphi = \varphi_0 + \gamma^{(1)}\frac{1}{g}(1-e^{-gL_1})P(L_1) + \gamma^{(2)}P(L_1)L_2$. Finally, $\mathcal{N} = \mathcal{N}_{\text{BC}}\mathcal{N}_{\text{evo}}$ governs the evolution of the perturbations over one roundtrip:

$$\begin{pmatrix} \hat{a}_{n+1}(0,\Omega) \\ \hat{b}_{n+1}(0,\Omega) \end{pmatrix} = \mathcal{N}(\Omega) \begin{pmatrix} \hat{a}_n(0,\Omega) \\ \hat{b}_n(0,\Omega) \end{pmatrix}. \tag{26}$$

If we denote the eigenvalues of $\mathcal{N}$ as $\lambda_{1,2}$, the MI gain in decibels per length reads

$$g(\Omega) = \frac{20}{L}\log_{10}\max\{|\lambda_1|, |\lambda_2|\}. \tag{27}$$

It is worth mentioning that a theoretical investigation of MI in a driven Kerr cavity containing an active medium has been performed in [18] using a meanfield model of the Lugiato-Lefever form. However, in our work we are considering a more general formalism based on evolution matrices, also involving the effect of gain saturation. Furthermore, at variance with [18] which investigates MI above the lasing threshold, we are using our model to investigate a different scenario with the cavity operating always below the lasing threshold and including a narrow band filter which is triggering the MI process.

4. Analytical and numerical results

Using Eq. (27), we show the dependency of MI gain on various parameters in Fig. 3(a)-Fig. 3(c). The horizontal dashed line in each figure indicates the parameter used in other two figures, while the vertical dashed lines indicate the filter center frequency. Figure 3(a) represents the evolution of MI gain versus unsaturated amplifier gain g_0. The setup consistently operates below the lasing threshold, specifically $\rho e^{\frac{gL_1}{2}} < 1$, as indicated by the red line at 5.7 dB/m. We observe two symmetric side lobes appearing on both sides of the pump and close to the filter center frequency, as in passive GTF cavities. Similar lobes also appear in Fig. 3(b), which shows the dependency of MI gain on the intracavity power P. In Fig. 3(c), the relationship between the MI gain and the linear phase shift φ_0 is presented. It clearly illustrates the influence of the filter on the MI gain, resulting in upward and downward tails around the filter center frequency. The evolution of the spectrum via simulation is shown in Fig. 3(d). The position of the first comb line, highlighted by the dashed vertical line, perfectly aligns with the position of the theoretically predicted highest MI gain indicated by the red dot in Fig. 3(c).

Figure 4 represents the output spectra for different amplifier gain values, when the input power is set at 1.0 W. By increasing the amplifier gain from 4.57 dB/m to 5.25 dB/m, we observe a broader spectral bandwidth and a greater number of comb lines generated. It is worth noting

Optics EXPRESS

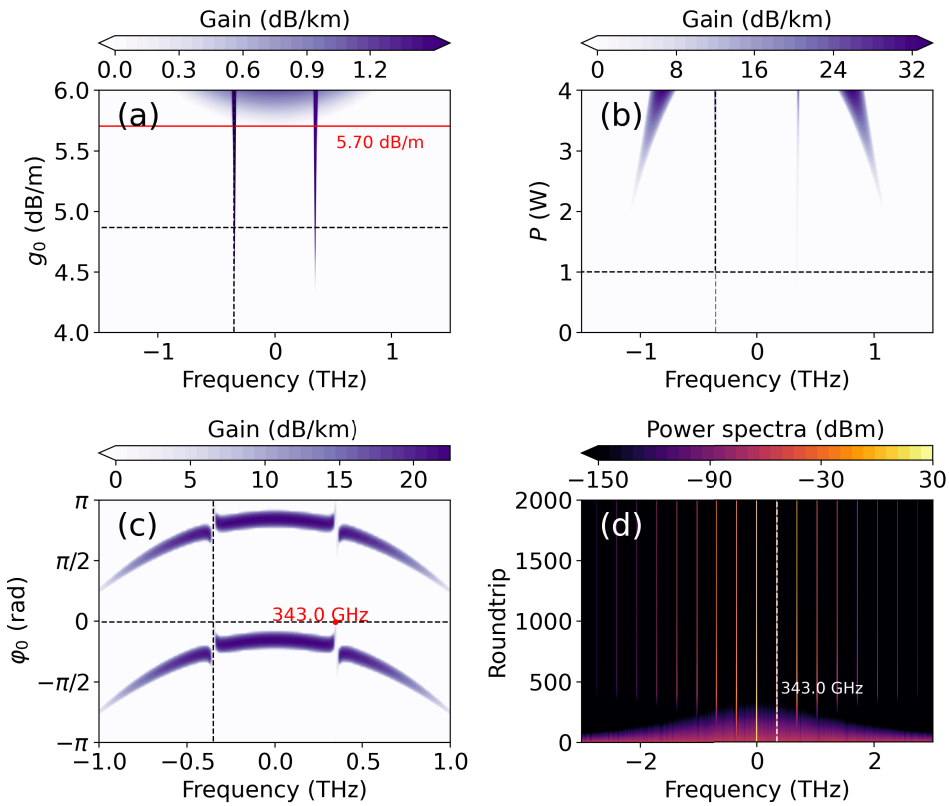

Fig. 3. MI gain map and simulations via Ikeda map. (a) MI gain versus g_0, the red solid line indicates $\rho e^{\frac{gL_1}{2}} = 1$. (b) MI gain versus intracavity power. (c) MI gain versus linear phase shift φ_0. (d) power spectrum evolution from simulations. Parameters used are $P = 1.0$ W, $\beta_2^{(1)} = -23$ ps^{2}km^{-1}, $\beta_2^{(2)} = 1.2$ ps^{2}km^{-1}, $\Omega_g/(2\pi) = 4$ THz, $\varphi_0' = -0.04$, and others are like Fig. 2.

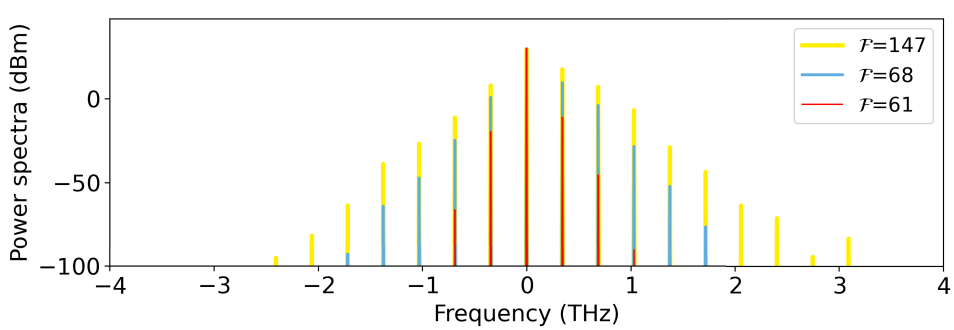

Fig. 4. Output spectra for various amplifier gain. Power spectrum with effective finesse being (a) $\mathcal{F} = 61$ ($g_0 = 4.55$ dB/m), (b) $\mathcal{F} = 68$ ($g_0 = 4.7$ dB/m), and (c) $\mathcal{F} = 147$ ($g_0 = 5.4$ dB/m). Parameters used are the same as those in Fig. 3, except that input power P_{in} is fixed at 1 W.

that a higher MI gain can lead to the generation of more spectral sidebands and hence a broader comb. However, when the MI gain becomes too large, the system tends to transition into a chaotic regime characterized by irregular amplitude and phase fluctuations, rather than forming a coherent and stable OFC. This inherent trade-off limits the extent to which bandwidth can be increased in the present scheme.

5. Experimental setup

We now describe the setup used for the experimental verification of the theoretical results described above. A schematic of the cavity is shown in Fig. 5(b). The main part of the cavity consists of 80 m of a DSF with a normal dispersion of $\beta_2^{(2)} = 1.2\ \mathrm{ps^2 km^{-1}}$. A 90/10 coupler is used to inject the signals into the cavity, while a 99/1 tap coupler is used to extract the signals. The filter used is a fiber Bragg grating (FBG) with a center wavelength of $\lambda_f = 1547.97$ nm, and it is fitted to the Lorentzian description given in Eqs. (2) with the parameters $a = 43$ rad/ns and $b = -1.06$. The amplifier consists of a piece of $L_2 = 0.33$ m erbium-doped fiber (EDF), which is connected to the passive fiber by two wavelength division multiplexers (WDMs). The pump of the EDF is a laser diode (LD) pump at 1490 nm injected through one of the WDMs. The use of the WDM allows the separation of the amplifier pump laser and the other useful signals. The complete setup is shown in Fig. 5(a). The laser pump is a CW tunable laser with a maximum output power of 44 mW and a linewidth of less than 100 Hz. The laser allows for fast tuning via an externally controllable piezo, which is used to stabilize the cavity, as explained below.

The pump is first divided into two parts by a 90/10 coupler, 90% for the strong driving signal and 10% for the control signal. The two signals are highlighted with a red and a blue path in the schematic. The driving signal is shaped into a pulse train using an intensity modulator (IM), driven by an arbitrary wave generator (AWG), with a pulse width of 1.3 ns and a repetition rate of $t_R = 451$ ns. The pulse train passes through an acousto-optic modulator (AOM). The AOM has a central operating frequency of 200 MHz and is driven by a signal generator (SG) that produces a sinusoidal signal. Adjusting the frequency of this signal allows one to fine-tune the frequency of the pump relative to the nearest cavity resonance. On top of that, the sinusoidal signal is gated synchronously with the pulses generated by the AWG, in order to exploit the 50 dB of extinction ratio of the AOM. This helps to increase the quality of the pulses and reduces the amount of noise amplified in the following steps. The signal is then amplified by a commercial EDFA and filtered (through BPF1) to suppress any residual spontaneous emission generated by the EDFA. A polarization controller (PC1) is used to align the signal to one of the polarization axes of the cavity, and an isolator is used to prevent any back reflection of the amplifier. Due to the high sensitivity of the cavity to external disturbances such as vibration, noise and temperature variations in the laboratory, a control loop is required to keep the drive signal in phase with the intracavity signal. The control system used in this experiment is an adaptation of the well-known Pound-Drever-Hall (PDH) technique [19], which requires a phase modulator (PM), a PDH controller and a proportional-integrative-derivative (PID) actuator to correct the laser frequency.

As shown by the blue path in the Fig. 5(a), 10% of the pump signal is modulated by the PM. The resulting signal passes through a chain consisting of an optical amplifier (OA), a filter (BPF2), a polarization controller (PC2) and an isolator, in a similar way to the driving signal, but at a much lower power to avoid any stimulated Brillouin scattering. After injection into the cavity, the signal is recovered at one of the outputs and converted into an electrical signal (black path) using a photodiode (PD1). This electrical signal is then processed by the PDH and the PID controller to produce a correction signal which is directly connected to the piezo-input of the laser pump. This signal constantly modifies the frequency of the pump, responding to any disturbances in the intracavity field and keeping the whole system coherent and stable.

Optics EXPRESS

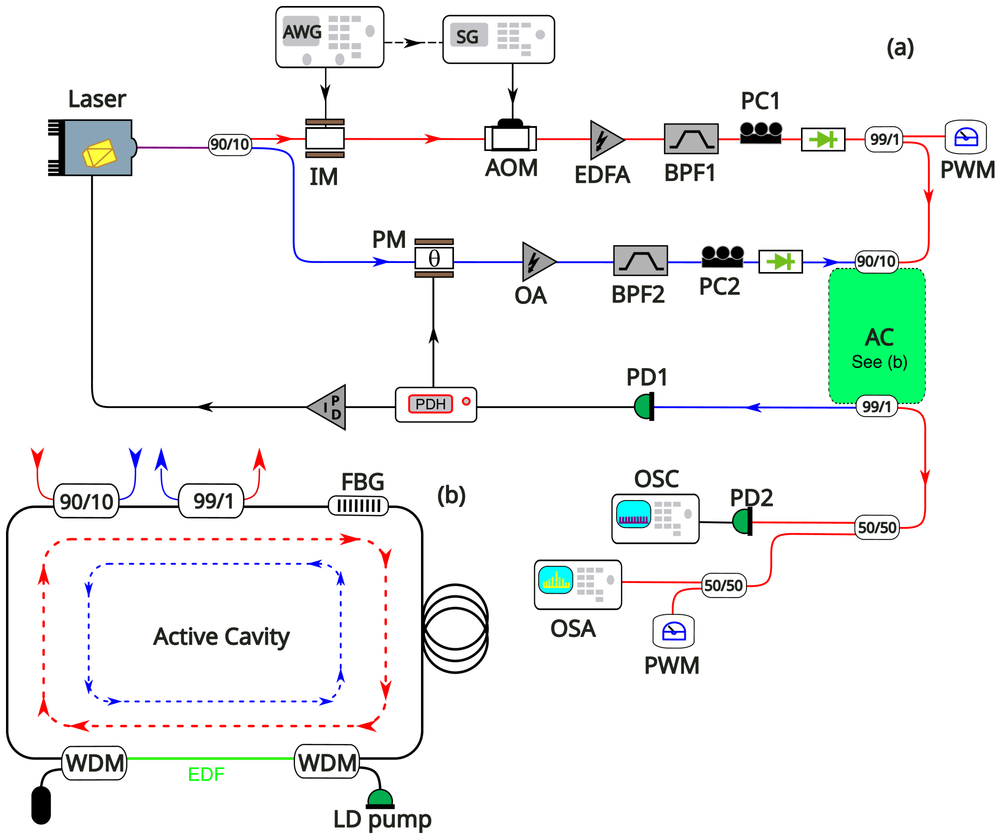

Fig. 5. Scheme of experimental setup and cavity (a) Experimental setup. IM: intensity modulator, AOM: acusto optical modulator, PM: phase modulator, EDFA: erbium-doped fiber amplifier, OA: optical amplifier, BPF1/2: band pass filters, PC1/2: polarization controllers. PDH: Pound-Drever-Hall module, PID: proportional-integrative-derivative controller. OSC: oscilloscope, OSA: optical spectrum analyzer, PWM: powermeters, AC: active cavity. (b) Scheme of the active cavity. LD pump: laser diode pump, WDM: wavelength division multiplexer, EDF: erbium-doped fiber, FBG: fiber Bragg grating. The red path indicates the route of the nonlinear signal, while the blue path indicates the route of the stabilization signal.

6. Experimental results

We have experimentally observed the spontaneous generation of spectral sidebands due to the GTF process in our system. We have explored the impact of the EDFA by recording different spectra as a function of different cavity finesse values obtained by varying the amplifier gain, by carefully keeping the cavity below the lasing threshold.

Figure 6 presents a comparison of spectra obtained from simulations and experiments for various input powers. The powers are all normalized to the zero mode. A good agreement between the simulations and experimental results is observed in both the comb line power and position, as illustrated in Fig. 6(c). Furthermore, an excellent agreement is noted regarding the input power threshold, as demonstrated in Fig. 6(a) and Fig. 6(b).

In Fig. 7, we present the dependency of the input power threshold to the amplifier gain. We observe that input pump power threshold for sidebands generation is reduced by increasing the amplifier gain. The experimental results are in good agreement with the numerical ones, where

Optics EXPRESS

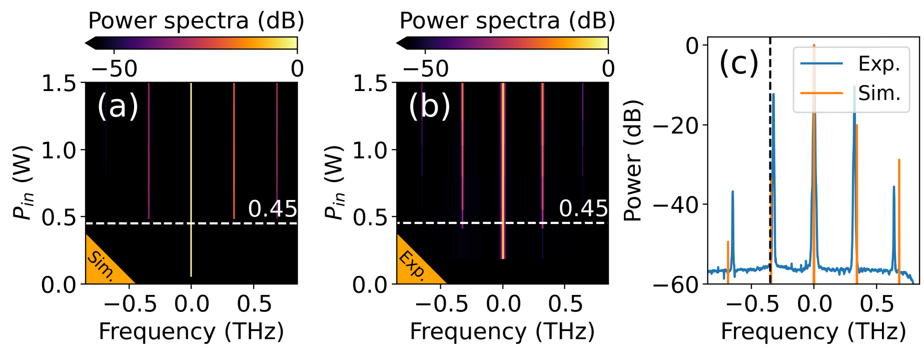

Fig. 6. Numerical and experimental power spectra. (a) Numerical spectra and (b) experimental spectra versus input pump power with g_0 = 4.76 dB/m. The dashed horizontal lines indicate the input power threshold. (c) Comparison of spectra between simulation and experiment for a selected input power power P_{in} = 1.36 W. The dashed vertical lines indicate the filter central frequency. Parameters used are like those in Fig. 3.

MI threshold corresponds to sidebands exceeding a power level of −72.5 dBm/Hz due to noise level. The analytical thresholds are instead determined by whether the MI gain is larger than 0, which does not account for the noise level, leading to a lower threshold.

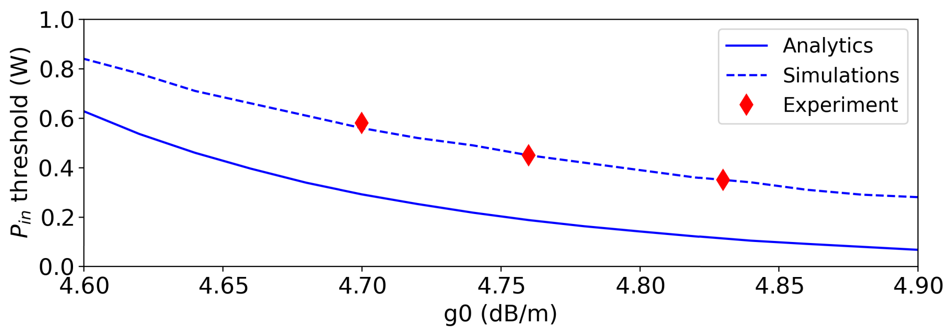

Fig. 7. Input power threshold versus amplifier gain obtain from analytics, numerics and experiments. Parameters used are like those in Fig. 3.

7. Conclusions

By integrating an EDFA into the GTF fiber cavity, and precisely adjusting the pump current to maintain the cavity below the lasing threshold, we successfully reduced the total losses increasing the resonator finesse. Consequently, we observed a decreased power threshold for GTF instability and enhanced energy transfer to spectral sidebands. These discoveries lay the foundations for advancing the efficiency and spectral bandwidth of GTF induced OFC sources.

Funding. Engineering and Physical Sciences Research Council (EP/W002868/1); Royal Academy of Engineering (Research Fellowship Scheme).

Disclosures. The authors declare no conflicts of interest.

Data availability. The datasets generated and analyzed during the current study are available from the corresponding author on reasonable request.

References

1. T. Fortier and E. Baumann, "20 years of developments in optical frequency comb technology and applications," Commun. Phys. **2**(1), 153 (2019).

Optics EXPRESS

2. A. M. Perego and A. Ellis, *Optical Frequency Combs, Trends in Sources and Applications* (CRC Press, 2024).
3. S. A. Diddams, K. Vahala, and T. Udem, "Optical frequency combs: Coherently uniting the electromagnetic spectrum," Science **369**(6501), 6501 (2020).
4. A. Parriaux, K. Hammani, and G. Millot, "Electro-optic frequency combs," Adv. Opt. Photonics **12**(1), 223–287 (2020).
5. A. Gaeta, M. Lipson, and T. Kippenberg, "Photonic-chip-based frequency combs," Nat. Photonics **13**(3), 158–169 (2019).
6. A. Perego, M. Conforti, A. Mussot, *et al.*, "Optical frequency combs in fibre resonators," in *Optical Frequency Combs. Trends in Sources and Applications*, A. M. Perego and A. D. Ellis, eds. (CRC Press, 2024), Chap. 7, pp. 153–174.
7. F. Leo, C. Coen, P. Kockaert, *et al.*, "Temporal cavity solitons in one-dimensional kerr media as bits in an all-optical buffer," Nat. Photonics **4**, 471–476 (2010).
8. D. Braje, L. Hollberg, and S. Diddams, "Brillouin-enhanced hyperparametric generation of an optical frequency comb in a monolithic highly nonlinear fiber cavity pumped by a cw laser," Phys. Rev. Lett. **102**(19), 193902 (2009).
9. T. Bunel, M. Conforti, Z. Ziani, *et al.*, "Observation of modulation instability kerr frequency combs in a fiber fabry–pérot resonator," Opt. Lett. **48**(2), 275–278 (2023).
10. T. Bunel, M. Conforti, Z. Ziani, *et al.*, "28 thz soliton frequency comb in a continuous-wave pumped fiber fabry–pérot resonator," APL Photonics **9**(1), 010804 (2024).
11. T. Bunel, J. Lumeau, A. Moreau, *et al.*, "Brillouin-induced kerr frequency comb in normal dispersion fiber fabry perot resonators," Nat. Commun. **16**(1), 5160 (2025).
12. T. Nie, K. Jia, Y. Xie, *et al.*, "Synthesized spatiotemporal mode-locking and photonic flywheel in multimode mesoresonators," Nat. Commun. **13**(1), 6395 (2022).
13. F. Bessin, A. M. Perego, K. Staliunas, *et al.*, "Gain-through-filtering enables tuneable frequency comb generation in passive optical resonators," Nat. Commun. **10**(1), 4489 (2019).
14. A. M. Perego, A. Mussot, and M. Conforti, "Theory of filter-induced modulation instability in driven passive optical resonators," Phys. Rev. A **103**(1), 013522 (2021).
15. N. Englebert, C. M. Arabí, P. Parra-Rivas, *et al.*, "Temporal solitons in a coherently driven active resonator," Nat. Photonics **15**(7), 536–541 (2021).
16. H. Bao, A. Cooper, M. Rowley, *et al.*, "Laser cavity-soliton microcombs," Nat. Photonics **13**(6), 384–389 (2019).
17. A. Haboucha, H. Leblond, M. Salhi, *et al.*, "Analysis of soliton pattern formation in passively mode-locked fiber lasers," Phys. Rev. A **78**(4), 043806 (2008).
18. M. Haelterman, S. Trillo, and S. Wabnitz, "Hopf sideband bifurcation and chaos in fiber lasers with injected signal," Phys. Rev. A **47**(3), 2344–2353 (1993).
19. E. D. Black, "An introduction to Pound–Drever–Hall laser frequency stabilization," Am. J. Phys. **69**(1), 79–87 (2001).